nature astronomy

Article https://doi.org/10.1038/s41550-022-01808-7

Imprints of cosmological tensions in reconstructed gravity

In the format provided by the authors and unedited

Supplemental Information: Imprints of cosmological tensions in reconstructed gravity

Levon Pogosian[1,2,3], Marco Raveri[4], Kazuya Koyama[2], Matteo Martinelli[5,6],
Alessandra Silvestri[7], Gong-Bo Zhao[3,8], Jian Li[1], Simone Peirone[7] & Alex Zucca[1]

I. ADDITIONAL INFORMATION ON THE FORMALISM, RECONSTRUCTION METHOD AND THE THEORY PRIOR

The starting point of our reconstruction is to parameterize Ω_X, μ and Σ in terms of their values at 11 discrete values (nodes) of a. From the 11 nodes, 10 values are distributed uniformly in the interval $a \in [1, 0.25]$ (corresponding to $z \in [0, 3]$) with another one at $a = 0.2$ ($z = 4$). We make the functions approach their ΛCDM values at higher redshifts, because the theoretical prior is obtained by looking at models that deviate from GR at late times only, though studying earlier times deviations from GR is generally possible within the same framework [1]. To allow for a smooth transition between their values at $z = 4$ and $z = 1000$, we add a set of 9 anchor nodes arranged along a tanh pattern, and then use cubic spline to interpolate between all the nodes to obtain continuous functions $\Omega_X(a)$, $\mu(a)$ and $\Sigma(a)$. Our results do not depend on how many nodes we use, since, with 10 nodes, we already include many nodes per prior correlation length and additional nodes will be made redundant by the correlation prior. In addition, the BAO, RSD, DES and SN data probe $z \lesssim 3$, while CMB constrains the integrated effect over $z \lesssim 1000$, with no data in the $3 < z < 1000$ range.

The cubic spline introduces an implicit smoothness prior into the reconstruction that suppresses sharp changes of the functions between nodes. Panel (a) of Fig. 1 shows the correlation between the nodes of Ω_X, μ and Σ imposed by the cubic spline. As one can see by comparing to Panel (b), this prior is substantially weaker than that derived from the Horndeski theories, as discussed below. Panels (c) and (d) show, respectively, the correlation imposed by data only (which includes the implicit prior), and by data in combination with the Horndeski prior.

We use an appropriately modified version of `MGCosmoMC`[1] [2–4], based on `CosmoMC`[2] [5], to sample the parameter space, which, in addition to the node parameters Ω_{Xi}, μ_i, Σ_i introduced earlier, includes the usual cosmological parameters: $\Omega_b h^2$, $\Omega_c h^2$, $\theta_\star$, τ, A_s, n_s, $\mathcal{N}$, where $\Omega_b h^2$ and $\Omega_c h^2$ are the physical densities of baryons and CDM, $\theta_\star$ is the angular size of the sound horizon at the decoupling epoch, τ is the reionization optical depth, A_s and n_s are the amplitude and the spectral index of primordial fluctuations, and $\mathcal{N}$ collectively denotes the nuisance parameters that appear in various data likelihoods. We note that the last node of Ω_X, corresponding to $a = 1$, is not varied as it is the same as the derived parameter $\Omega_{\rm DE}$. We run 8 MCMC chains and assess their convergence through the Gelman-Rubin criterion, assuming the chains have reached convergence when $R - 1 \lesssim 0.1$ for the least converged eigenvalue, ensuring that all others have a higher degree of convergence ($R - 1 \sim 0.01$).

In addition to performing the reconstruction of $\Omega_X(a)$, $\mu(a)$ and $\Sigma(a)$ by determining the best fit node parameters from data alone, we use the method of [6, 7] to add the Horndeski prior that correlates the nodes $\{\Omega_{Xi}, \mu_i, \Sigma_i\} \equiv \mathbf{f}$. It is introduced as a Gaussian prior

$$\mathcal{P}_{\rm prior} \propto \exp[-(\mathbf{f} - \mathbf{f}_{\rm fid})\mathcal{C}^{-1}(\mathbf{f} - \mathbf{f}_{\rm fid})^T] \,, \qquad (1)$$

where $\mathcal{C}$ is the correlation matrix derived from the joint covariance of the three functions obtained in [8]. While we have the full covariance at our disposal, along with the mean values, we opt not to use the latter as our fiducial values $\mathbf{f}_{\rm fid}$ in order to avoid biasing the outcome of the reconstruction, and also use the normalized correlation matrix for $\mathcal{C}$. In practice, the prior is implemented as a new contribution to the total χ^2, with $\mathbf{f}_{\rm fid}$ determined during sampling using the so-called "running average" method [6]. The theory prior acts much like a Wiener filter, discouraging (but not completely prohibiting) abrupt variations of the functions.

Panel (b) of Fig. 1 shows the Horndeski correlation prior used in our work. One can clearly see that the correlation "length" is much longer than that of the implicit prior due to the cubic spline shown in Panel (a). This ensures that the prior aided reconstruction is independent of the binning scheme. Also notable is the nearly perfect correlation between μ and Σ, in line with the $(\Sigma - 1)(\mu - 1) \geq 0$ conjecture made in [9]. The correlation between Ω_X and μ or Σ is nearly absent, although, as mentioned above, it can be strong in certain subclasses of Horndeski theories.

We do not consider the k-dependence of μ and Σ, focusing solely on their evolution with redshift. This helps to reduce the computational costs and is largely justified by the fact that, in practically all known MG theories, the scale-dependence of these functions manifests itself outside the range of linear scales probed by large scale structure (LSS) surveys [10, 11]. Most of the previous cosmological tests of GR have focused on separately testing either the background expansion or modified growth and/or employed simple *ad hoc* parameterizations of w, μ and Σ, or their equivalents [12], which can bias the results and prevent capturing important information in

[1] https://github.com/sfu-cosmo/MGCosmoMC
[2] http://cosmologist.info/cosmomc/

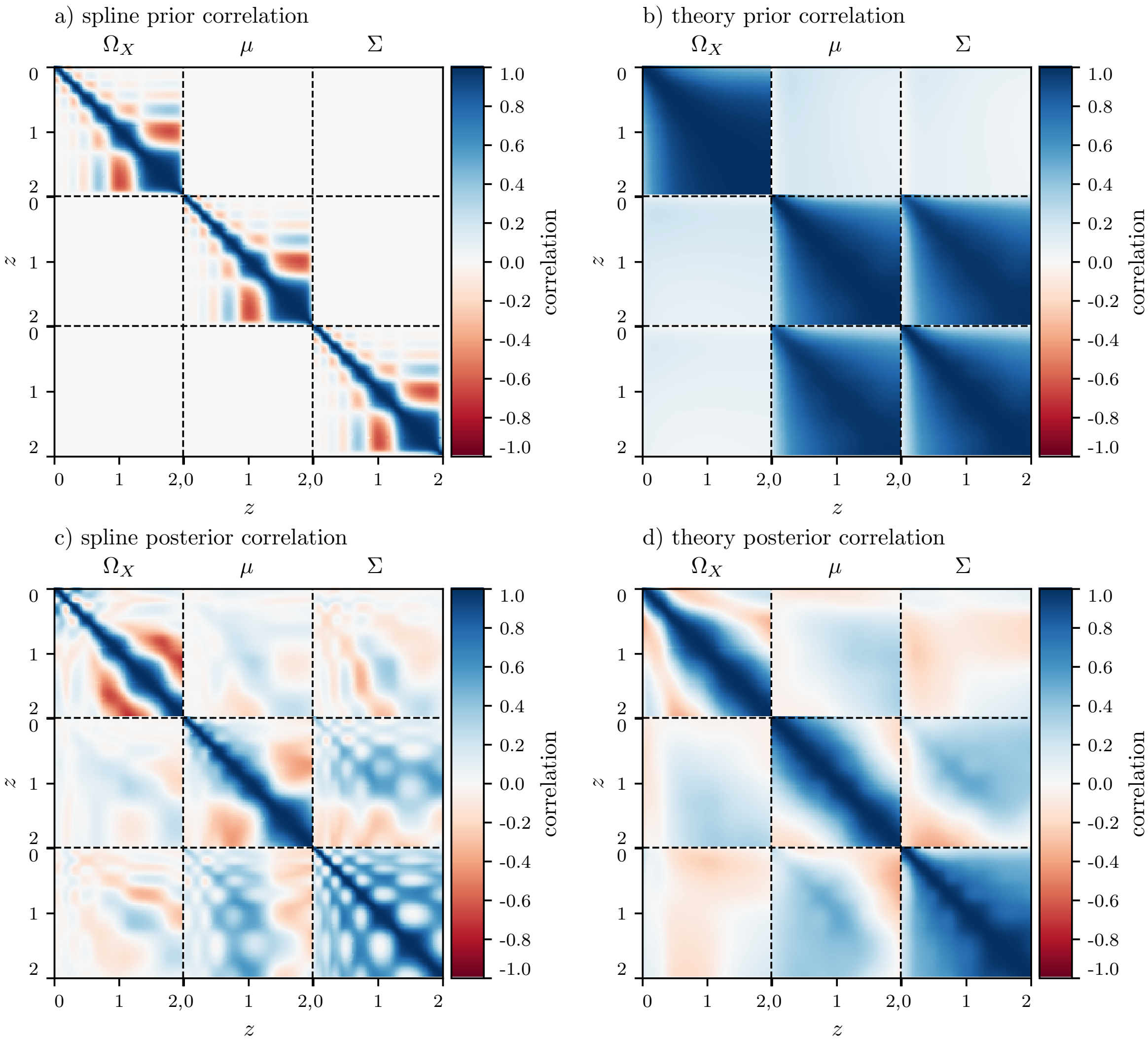

FIG. 1. a) The implicit correlation prior, as a function of redshift, induced by using the cubic spline to connect the 11 redshift nodes. All three functions, Ω_X, μ and Σ, are subject to the same implicit prior, with no cross-correlation between different functions. b) The Horndeski prior correlating the nodes of Ω_X, μ and Σ. The correlation between the nodes of each function is much stronger than that introduced by the cubic spline. The Horndeski prior also introduces a strong correlation between μ and Σ. c) The correlation obtained from our "Baseline" data posterior covariance of the nodes, *i.e.* that determined by the data and the implicit prior correlation in Panel (a). d) The correlation corresponding to the posterior covariance derived from the Baseline data with the help of the Horndeski prior in Panel (b).

the data, as demonstrated in [13]. We note that three functions equivalent to Ω_X, μ and Σ were reconstructed in [14] from the so-called "observables" [15], or model-independent combinations of the data, with a particular focus on constraining the gravitational slip γ. While very interesting, the methods in that work did not allow determination of the cosmological parameters and addressing the tensions, nor considered the effect of correlations between the functions that could come from theory. A reconstruction of the free functions in the effective theory description of Horndeski [16, 17] was performed using a similar method in [18, 19], showing interesting hints of departures from GR, albeit at low statistical significance. Our reconstruction has the benefit of not being restricted to Horndeski theories, while still allowing us to check the consistency of various subclasses of Horndeski theories with the data.

We restricted our studies to late-time modifications of ΛCDM because there one can make a clear connection to the theoretical predictions in the quasi-static limit, and also because extending our phenomenological approach to earlier times would require making additional assumptions about the effect of modified gravity on radiation, which makes the framework less generic. In [1], a similar phenomenological parametrization was used to study effects of modified gravity at times around recombination, finding that this could help to ease the H_0 tensions. Also, in [20], a reconstruction of the dark energy density was performed using methods similar to ours, finding that this can resolve the Hubble tension, but not the S_8 tension.

II. ADDITIONAL INFORMATION ON DATASETS

We consider combinations of the following datasets:

- "Planck": the 2018 release of the Planck CMB temperature, polarization and the reconstructed CMB weak lensing spectra [21];
- "BAO": the eBOSS DR16 BAO compilation from [22] that includes measurements at multiple redshifts from the samples of Luminous Red Galaxies (LRGs), Emission Line Galaxies (ELGs), clustering quasars (QSOs), and the Lyman-α forest [23–26], along with the SDSS DR7 MGS [27] data. We also add the BAO measurement from 6dF [28]. This compilation covers the BAO measurements at $0.07 < z < 3.5$. Note that the BAO data considered here are the "tomographic" version of the DR12 BOSS BAO at $0.20 < z < 0.75$ [29] (not the "consensus" version using effective redshifts presented in [22]).
- "SN": the Pantheon SN sample at $0.01 < z < 2.3$ [30];
- "RSD": the eBOSS joint measurement of BAO and RSD for LRGs, ELGs and QSOs [25, 31–33], using it instead of the eBOSS BAO-only measurement. For LRGs, it combines eBOSS LRGs and BOSS CMASS galaxies spanning the redshift range $0.6 < z < 1$, at an effective redshift of $z_{\rm eff} = 0.698$. QSOs cover $0.8 < z < 2.2$ with an effective redshift of $z_{\rm eff} = 1.48$, while ELGs cover $0.6 < z < 1.1$ with an effective redshift of $z_{\rm eff} = 0.845$. In addition, we add BAO-only measurements from 6dF and MGS.
- "DES": the Dark Energy Survey Year 1 measurements of the angular two-point correlation functions of galaxy clustering, cosmic shear and galaxy-galaxy lensing with source galaxies at $0.2 < z < 1.3$ [34]; since our formalism has no nonlinear prescription for structure formation, the angular separations probing the nonlinear scales were removed using the "aggressive" cut option of `MGCAMB` described in [4], which uses the method introduced in [12, 34].
- "'$\mathrm{M_{SN}}$": the SH0ES determination of the intrinsic SN type Ia brightness magnitude as obtained by [35], included in the Pantheon SN likelihood as in [36]. This provides a measurement of $H_0 = 73.2 \pm 1.3$ km/s/Mpc in ΛCDM.

Our baseline dataset combination (labelled "Baseline" from now on) includes Planck, BAO and SN. In addition, we also consider the additional Baseline+RSD+DES and Baseline+RSD+DES+$\mathrm{M_{SN}}$. Note that, when RSD is included in the combination, the BAO data do not coincide with the one used in Baseline for the eBOSS LRGs BAO measurement, as we replace it with the joint RSD-BAO measurement. We note that a non-linear modelling of RSD is required to extract the linear growth rate $f\sigma_8$, which was done assuming ΛCDM. In principle, there can be additional non-linear effects from modified gravity that could bias the ΛCDM-based extraction of $f\sigma_8$. For specific modified gravity models with the scale independent growth, this bias was shown to be negligible for current measurements [37]. However, this conclusion depends on the theory of gravity as well as the accuracy of the measurements [38].

For brevity, we refer to RSD+DES as simply "LSS", and to Baseline+RSD+DES+$\mathrm{M_{SN}}$ as "All".

III. EXTENDED ANALYSIS OF COSMOLOGICAL TENSIONS

Including the lensing amplitude $A_{\rm L}$ [39] as an extra free parameter helps to assess if the high redshift departure of $\Sigma(z)$ from the GR limit is indeed due to the CMB lensing anomaly. This is a completely phenomenological parameter that rescales the contribution of weak gravitational lensing to the CMB temperature anisotropy spectrum (TT). In a self-consistent cosmological model one should have $A_{\rm L} = 1$. Fig. 2 shows the reconstruction of $\Sigma(z)$ with and without the correlation prior, for both the Baseline and Baseline+LSS data combinations, and with the $A_{\rm L}$ parameter both fixed to unity and free to vary. Comparing the fixed and free $A_{\rm L}$ reconstructions shows how the inclusion of $A_{\rm L}$ completely removes the high z departure from GR, with $\Sigma(z)$ now fully consistent with one.

We further explore the correlations between $\Sigma(z)$ and $A_{\rm L}$ and its implication for the S_8 parameter in Fig. 3. As discussed in the main text, the reconstructed shapes of Ω_X and μ allow for slightly lower values of S_8 than ΛCDM. However, S_8 is also related to the amplitude of the lensing potential, which in our analysis is modulated by Σ. The parameter that is constrained by DES is $\langle\Sigma\rangle S_8$ where $\langle\Sigma\rangle$ is an average of Σ in the redshift range relevant for DES, and it is equal to one in the ΛCDM limit. Despite the lowering of S_8, this parameter remains the same as that in ΛCDM when $A_{\rm L} = 1$, as it can be seen in the top panels of Tables I and II, where the results for this case are shown. This is due to the enhancement of Σ from the GR limit driven by the CMB lensing anomaly as discussed above. As a consequence, if one keeps a fixed $A_{\rm L} = 1$, the quality of the fit to DES data is not better than ΛCDM even when Ω_X, μ and Σ are free to vary (see Table II). If one instead allows for $A_{\rm L}$ to be free, an anomalous value of this parameter "solves" the CMB lensing anomaly, and Σ becomes consistent with the GR limit. In this case, the lowering of S_8 leads to lower values

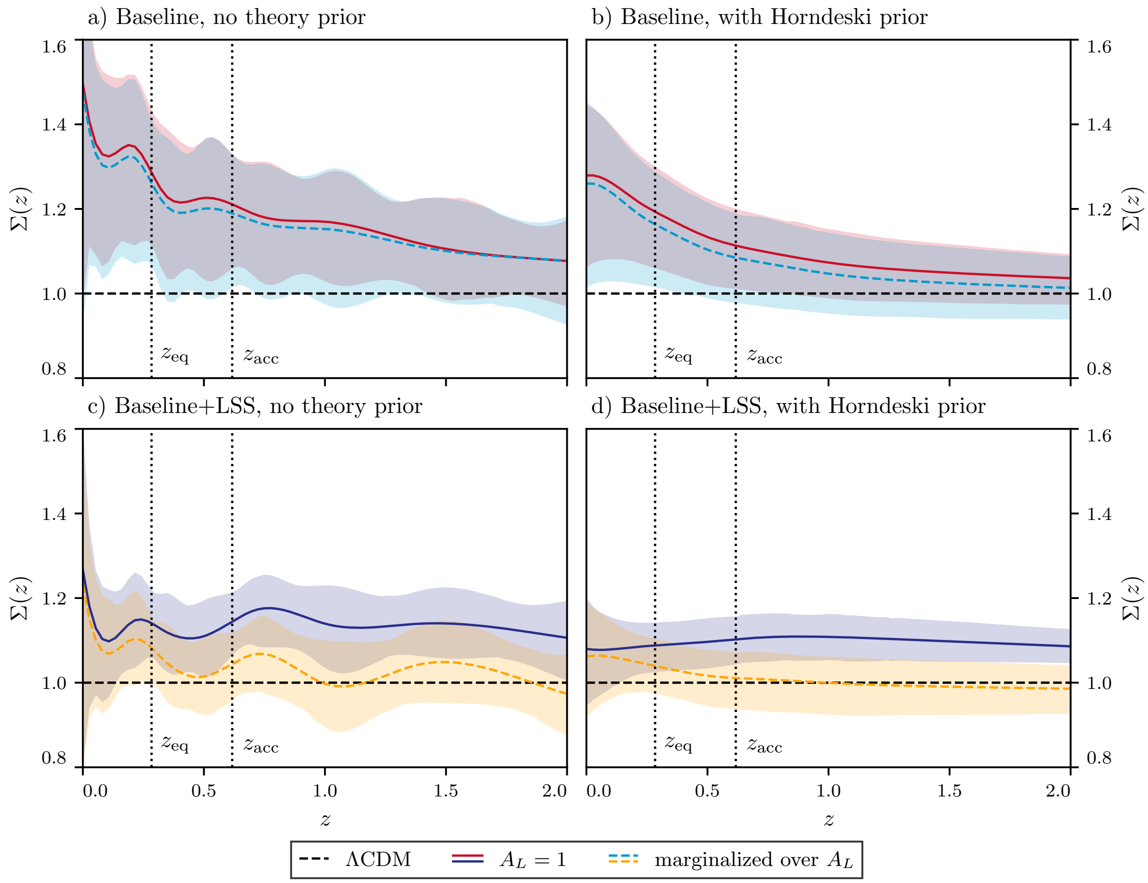

FIG. 2. Reconstruction of $\Sigma(z)$ from the Baseline (top panels) and the Baseline+LSS (bottom panels) data combinations, without (left panels) and with adding the Horndeski correlation prior (right panels). Solid lines show the reconstructed mean values with the lensing amplitude parameter $A_{\rm L}$ fixed to unity, while the dashed lines correspond to the case where $A_{\rm L}$ was free to vary. The shaded regions show the corresponding 68% confidence levels.

of $\langle\Sigma\rangle S_8$ and the fit to the DES data is improved compared with ΛCDM. Table II shows the values of the χ^2 for the different data considered in the analysis. One can see that, with respect to ΛCDM, the $A_{\rm L} = 1$ analysis improves the DES χ^2 by 0.4 (1.2 without the Hordenski prior), while this improvement increases to 2.8 (4.7 without the Hordenski prior) if $A_{\rm L}$ is free. Overall, this analysis reveals that the late time modifications alone are not able to improve the fit to CMB and DES weak lensing simultaneously.

We now turn our attention to the impact of including the SH0ES prior on the SN magnitude in the data combination analyzed. As it can be seen in Table III, the main impact of such an addition is an enlargement of the uncertainties and an increase of the estimated mean value of H_0. We find $H_0 = 69.44 \pm 1.30$ km/s/Mpc, which is consistent with the value obtained by SH0ES within 2σ. Fig. 4 shows Ω_m, H_0 and the sound horizon at baryon decoupling $r_{\rm drag}$, with and without the SH0ES prior and with and without the Horndeski prior. It is possible to notice how, for the Baseline+LSS combination, the additional freedom given by the Ω_X, μ and Σ functions only produces an enlargement of the error on H_0, with its mean value being the same as in ΛCDM. When the SH0ES prior is included we obtain instead the increase of the mean value of H_0 as well as a slight shift of $r_{\rm drag}$ with respect to ΛCDM.

Fig. 4 of the Article shows the difference of the luminosity distance prediction with the SH0ES prior from the prediction of the best-fit ΛCDM without the SH0ES prior. The Pantheon SN data points are calibrated using the SH0ES measurement of $M_{\rm SN}$ while the BAO data points are converted to the luminosity distance from the angular diameter distance using $d_L = (1+z)^2 d_A$. There are two main issues. The first problem is that the luminosity distance calibrated from CMB in ΛCDM does not agree with the SN data while it agrees with the BAO data. The second problem is the discrepancy between the BAO and SN data. The latter makes it hard for late modifications to resolve this tension fully as it is not possible to fit BAO and SN data simultaneously unless we change $r_{\rm drag}$ by an early time modification. This is also the case in our reconstruction. Due to the freedom in $\Omega_X(z)$, the luminosity distance at lower redshifts

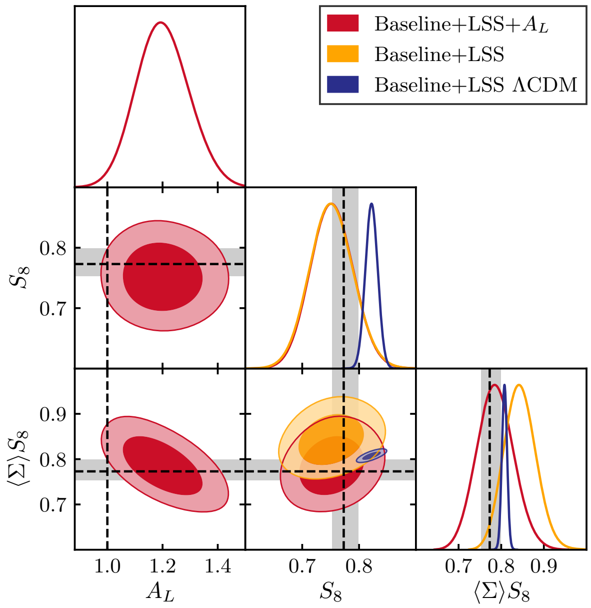

FIG. 3. The 68% and 95% confidence level contours for the parameters $A_{\rm L}$, S_8 and the combination $\langle\Sigma\rangle S_8$ derived from the Baseline+LSS data with the Horndeski prior. Yellow contours refer to the case where $A_{\rm L} = 1$, while the red contours represent the case with $A_{\rm L}$ being a free parameters. The blue contours show the ΛCDM fit to Baseline+LSS. The grey bands show the constraints on S_8 and $\langle\Sigma\rangle S_8$ obtained by DES in the ΛCDM model, in which $\langle\Sigma\rangle = 1$.

becomes closer to the SN data compared with ΛCDM, which leads to a larger H_0. However, it is still not possible to reproduce the luminosity distance calibrated by the SH0ES measurement of $M_{\rm SN}$ fully.

To show the extent to which the well known H_0 and S_8 tensions can be resolved by allowing for time-dependent Ω_X, μ and Σ, we show in Fig. 5 the constraints on Ω_m, H_0 and $\langle\Sigma\rangle S_8$ and compare the results obtained with and without the SH0ES prior. The results shown in this figure refer to the case where $A_{\rm L}$ is considered as a free parameter. As discussed before, without this parameter, the CMB lensing would prevents us from addressing the S_8 tension, thus achieving a better fit to DES. On the other hand, allowing for a varying A_L removes the CMB anomaly, making it possible to fit simultaneously to the SH0ES and DES data better than ΛCDM. As shown in Table III, the total improvement of χ^2 is $\Delta\chi^2 = -25.8$ without the Horndeski prior and $\Delta\chi^2 = -14.1$ with the prior.

IV. EXTENDED DISCUSSION OF IMPLICATIONS FOR HORNDESKI

Any statistically significant departure of $X(z)$, $\mu(z)$ or $\Sigma(z)$ from unity would imply either a break down of the ΛCDM model or a problem, *e.g.* a systematic effect, with some of the datasets. The deviations from the ΛCDM prediction seen in our reconstructions are at a level of $\sim 2\sigma$, comparable to the significance of the S_8 and A_L tensions. While this hardly prompts an urgent revision of ΛCDM, it is nevertheless interesting to ask what implications the trends exhibited by the reconstructions would have for alternative models. In what follows, we first interpret the reconstruction results in the context of Horndeski theories, showing that the reconstructed evolution of the three functions, had it been detected at a higher confidence level, would rule out broad classes of scalar-tensor theories.

As shown in [40], under the QSA, the expressions for μ and Σ in local theories of gravity take the form of ratios of polynomials in k. In Horndeski theories, with second order equations of motion, the polynomials are quadratic in k. The scale dependence of μ and Σ, however, is unlikely to manifest itself in the range of k probed by large scale structure surveys for which linear perturbation theory is valid. The k-dependence marks the transition from the $k \ll \lambda_f^{-1}$ limit, where perturbations of the scalar field can be neglected, to the $k \gg \lambda_f^{-1}$ regime in which the scalar field perturbations mediate a fifth force. The known screening mechanisms in Horndeski theories place the range of k probed by our reconstruction in one of these two limits [10, 11].

While the QSA is not guaranteed to be accurate in all circumstances, especially on near-horizon scales, it has been found to work quite well for identifying the key phenomenological signatures of Horndeski theories [41]. Even though we cannot be certain which regime, $k \ll \lambda_f^{-1}$ or $k \gg \lambda_f^{-1}$, is being probed by our scale-independent parametrization, we can still make several useful deduction by comparing our reconstructions to the QSA expressions for μ and Σ in the two limits.

In the $k \ll \lambda_f^{-1}$ limit, the QSA expressions for our functions are [9]

$$\mu \to \mu_0 = \frac{m_0^2}{M_\star^2} c_T^2 \tag{2}$$

$$\Sigma \to \Sigma_0 = \frac{m_0^2}{M_\star^2} \frac{1+c_T^2}{2} \tag{3}$$

$$\gamma \to \gamma_0 = c_T^{-2} \; , \tag{4}$$

while, for $k \gg \lambda_f^{-1}$, one has [9, 42]

$$\mu \to \mu_\infty = \frac{m_0^2}{M_\star^2}(c_T^2 + \beta_\xi^2) \tag{5}$$

$$\Sigma \to \Sigma_\infty = \frac{m_0^2}{M_\star^2}\left(\frac{1+c_T^2}{2} + \frac{\beta_\xi^2 + \beta_B\beta_\xi}{2}\right) \tag{6}$$

$$\gamma \to \gamma_\infty = \frac{1+\beta_B\beta_\xi}{c_T^2 + \beta_\xi^2} \; , \tag{7}$$

where m_0 is the Planck mass, $M_\star$ is the modified Planck mass, c_T is the propagation speed of tensor metric modes, *i.e.* the speed of gravitational waves, while β_B and β_ξ are two functions, originating from different ways of coupling

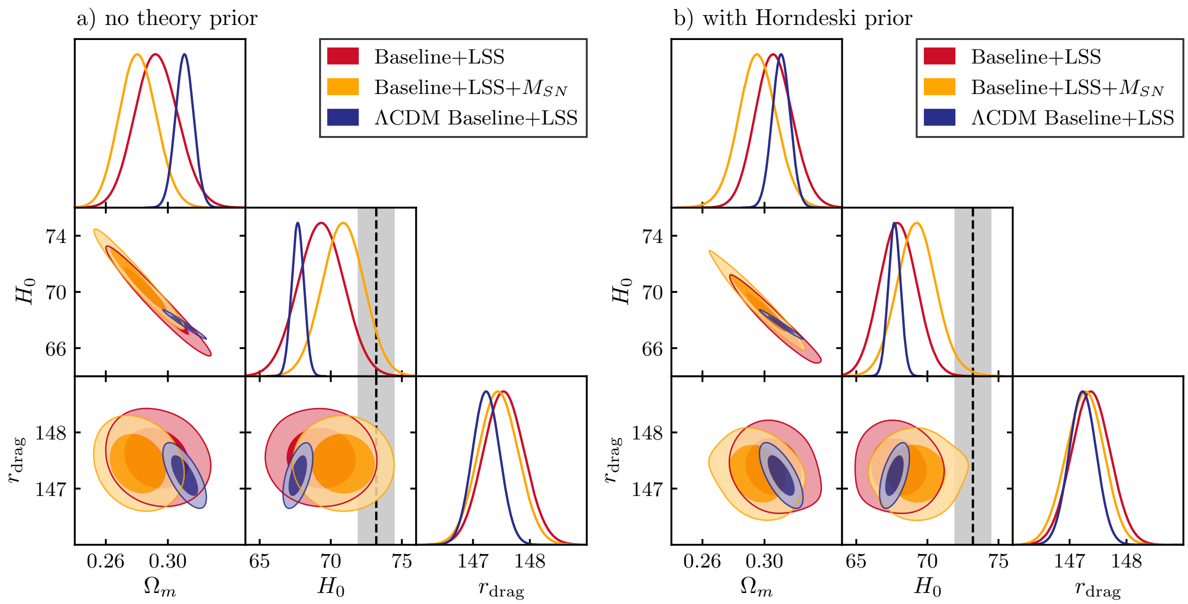

FIG. 4. 68% and 95% confidence level contours Ω_m, H_0 and the sound horizon at baryon decoupling $r_{\rm drag}$, with and without the SH0ES prior (yellow and red contours, respectively) and with and without the Horndeski prior (left and right panels, respectively). The blue contours show the ΛCDM fit to Baseline+LSS, while the grey band shows the constrain on H_0 obtained by the SH0ES collaboration.

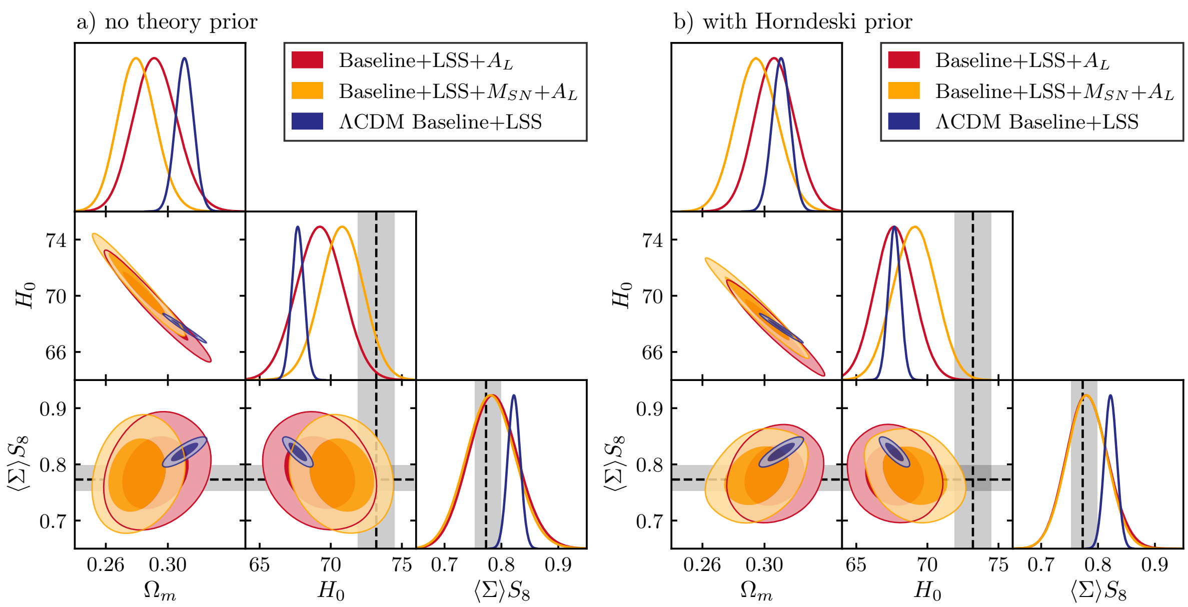

FIG. 5. The 68% and 95% confidence level contours for the tension parameters, S_8, H_0 and Ω_M, from the Baseline+LSS data with and without the SH0ES prior on the SN magnitude $\mathrm{M_{SN}}$ (yellow and red contours, respectively), and with and without the Horndeski prior (left and right panels, respectively). The blue contours show the results obtained in the ΛCDM limit, while the grey band shows the H_0 measured by the SH0ES collaboration.

the metric and the scalar field, that represent the fifth force contribution.

The limiting expressions above highlight the close relationship between the gravitational slip and the tensor speed c_T [43]. In particular, γ must approach 1 in the large scale limit if $c_T = 1$ [9]. In the small scale limit, on the other hand, $\gamma \neq 1$ could be either due to a fifth force or $c_T \neq 1$, or both. Since $c_T \neq 1$ is disfavoured by the multi-messenger observations of gravitational waves from binary neutron stars at $z \sim 0$ [44, 45], one would

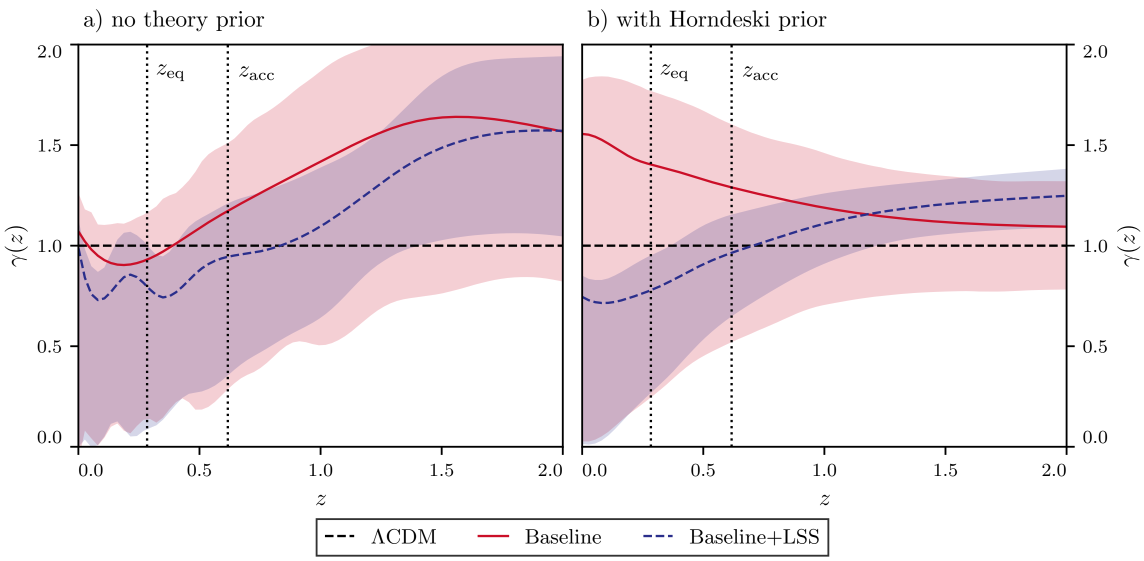

FIG. 6. Reconstruction of the gravitational slip $\gamma(z)$ constructed from $\mu(z)$ and $\Sigma(z)$. The reconstruction is obtained using only data (left panel) and adding the Horndeski correlation prior (right panel). Red lines show the mean reconstructions using the Baseline data combination, with the red region showing the 68% confidence level, while blue lines and regions refer to the case where RSD and DES are added to the baseline.

conclude that there is evidence for a fifth force at low redshifts.

The subclass of the Horndeski theories with $\gamma = 1$, other than ΛCDM, include the Cubic Galileon [46] and KGB [47] models, along with the so-called "no-slip gravity" [48], for which $c_T = 1, \beta_\xi = 0$ so that

$$\mu_0 = \Sigma_0 = \mu_\infty = \Sigma_\infty = \frac{m_0^2}{M_*^2}. \tag{8}$$

Fig. 6 shows the gravitational slip $\gamma(z)$ derived from the reconstructions of $\mu(z)$ and $\Sigma(z)$. It is important to note that the Baseline dataset is not capable of breaking the degeneracy between μ and Σ. Correspondingly, $\gamma(z)$ reconstructed from the Baseline data has a large uncertainty and is strongly prior dependent. Using Baseline+RSD+DES, on the other hand, allows for the degeneracy between $\mu(z)$ and $\Sigma(z)$ to be partially broken. As a result, $\gamma(z)$ is better constrained and the trends in its time-evolution are essentially the same with and without the Horndeski prior. In both cases, one finds $\gamma > 1$ at higher z and $\gamma < 1$ at lower z, with the transition between these two limits happening around the redshift at which cosmic acceleration sets in. In the case with the Horndeski prior, the uncertainties are reduced, making the trend significant at more than 2σ.

Keeping in mind that the significance of the $\gamma \neq 1$ detection is relatively low, one could ask what such a time-dependence would imply for Horndeski theories. Aside from ruling out models with $\gamma = 1$, like the no-slip gravity, Cubic Galileons and KGB, the fact that we observe $\gamma > 1$ would rule out the generalized Brans-Dicke models (GBD), which predicts $c_T = 1$ and $\beta_B = -\beta_\xi$, *i.e.* all models with a canonical form of the scalar field kinetic energy term. The latter conclusion follows from the fact that one should have $\gamma \leq 1$ in GBD on all scales.

Finally, as pointed out in [9] based on analytical considerations in the QSA limit, and later confirmed by a numerical sampling of Horndeski solutions [8, 41], one expects a strong correlation between μ and Σ, with $(\Sigma - 1)(\mu - 1) \geq 0$. To violate the latter condition, independent sectors/terms of the Horndeski theory would need to conspire to evolve in just the right way for no apparent reason. Thus, looking for signs of violation of the $(\Sigma - 1)(\mu - 1) \geq 0$ conjecture is an important test of Horndeski. Fig. 7 shows the evolution of $(\Sigma - 1)(\mu - 1)$ derived from our reconstructions. With or without the Horndeski prior, the reconstructions show a good consistency with $(\Sigma - 1)(\mu - 1) \geq 0$.

V. PARAMETER TABLES

[1] Lin, M.-X., Raveri, M. & Hu, W. Phenomenology of Modified Gravity at Recombination. *Phys. Rev. D* **99**, 043514 (2019). 1810.02333.

[2] Zhao, G.-B., Pogosian, L., Silvestri, A. & Zylberberg, J. Searching for modified growth patterns with tomographic surveys. *Phys. Rev.* **D79**, 083513 (2009). 0809.3791.

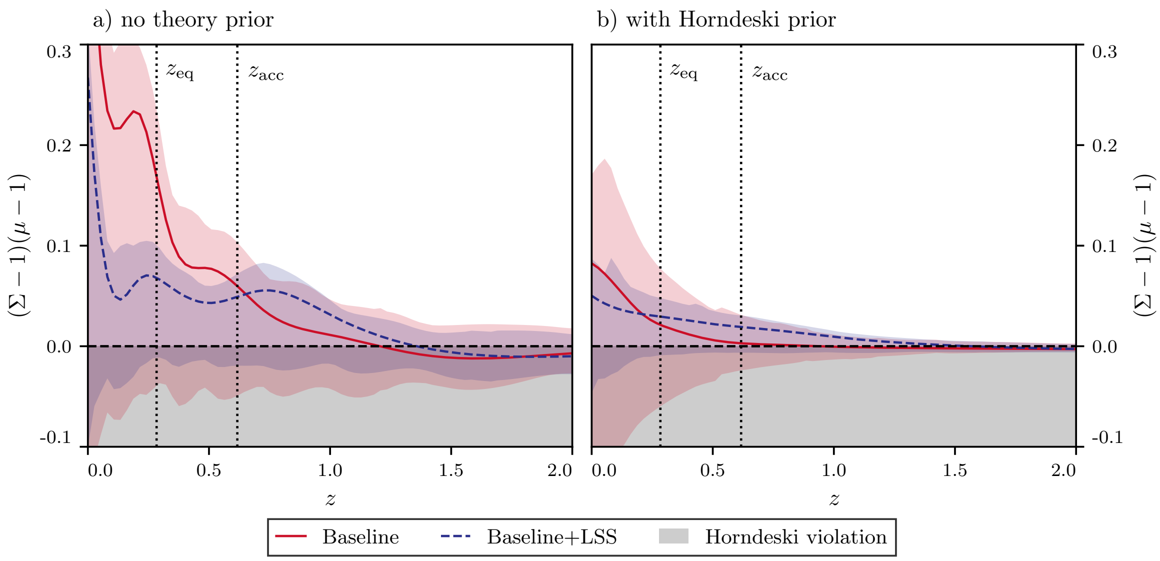

FIG. 7. Reconstruction of the combination $(\Sigma(z)-1)(\mu(z)-1)$, with red lines/regions corresponding to the mean/68% confidence level for the Baseline data combination, and blue lines/regions representing the case where RSD and DES are added to the Baseline. The gray region shows the area where the Horndeski conjecture is violated.

Baseline data	ΛCDM (reference)	No theory prior	With Horndeski prior
H_0	$(67.44)\,67.43^{+0.78}_{-0.81}$	$(69.86)\,69.2\pm1.4$	$(67.70)\,67.6^{+1.4}_{-1.2}$
Ω_m	$(0.3141)\,0.314^{+0.011}_{-0.011}$	$(0.2890)\,0.295\pm0.012$	$(0.3108)\,0.310^{+0.010}_{-0.014}$
$\langle\Sigma\rangle S_8$	$(0.8319)\,0.831^{+0.021}_{-0.020}$	$(0.8529)\,0.893\pm0.050$	$(0.8555)\,0.901\pm0.044$
$\chi^2_{\rm CMB}$	2765.7	$2760.7\,(-5)$	$2761.92\,(-3.8)$
$\chi^2_{\rm CMBL}$	8.7	$9.9\,(+1.2)$	$9.58\,(+0.9)$
$\chi^2_{\rm SN}$	1035.2	$1030.9\,(-4.3)$	$1035.5\,(+0.3)$
$\chi^2_{\rm BAO}$	20.6	$15.3\,(-5.3)$	$21.08\,(+0.5)$
$\chi^2_{\rm tot}$	3830.2	$3816.9\,(-13.3)$	$3828.1\,(-2.1)$
	ΛCDM $+A_L$	No theory prior $+A_L$	With Horndeski prior $+A_L$
H_0	$(67.896)\,67.83\pm0.46$	$(69.78)\,69.3\pm1.4$	$(67.15)\,67.8^{+1.1}_{-1.4}$
Ω_m	$(0.3079)\,0.3088\pm0.0061$	$(0.2902)\,0.294^{+0.011}_{-0.013}$	$(0.3122)\,0.308\pm0.012$
$\langle\Sigma\rangle S_8$	$(0.8114)\,0.814\pm0.013$	$(0.800)\,0.883^{+0.067}_{-0.081}$	$(0.817)\,0.870\pm0.070$
A_L	$(1.0739)\,1.069\pm0.036$	$(1.084)\,1.027^{+0.093}_{-0.11}$	$(1.117)\,1.060^{+0.093}_{-0.13}$
$\chi^2_{\rm CMB}$	$2760.2\,(-5.5)$	$2759.9\,(-5.8)$	$2759.6\,(6.1)$
$\chi^2_{\rm CMBL}$	$10.0\,(+1.3)$	$9.7\,(+1.0)$	$9.7\,(+1.0)$
$\chi^2_{\rm SN}$	$1034.9\,(-0.3)$	$1030.8\,(-4.4)$	$1035.7\,(+0.5)$
$\chi^2_{\rm BAO}$	$21.0\,(+0.4)$	$15.7\,(-4.9)$	$20.1\,(-0.5)$
$\chi^2_{\rm tot}$	$3826.1\,(-4.1)$	$3816.2\,(-14.0)$	$3825.1\,(-5.1)$

TABLE I. The best fitting maximum posterior model parameters, in parentheses, mean and 68% C.L. constraints for the *Baseline* data combination. Data likelihoods at maximum posterior are compared to their reference ΛCDM values in parenthesis.

[3] Hojjati, A., Pogosian, L. & Zhao, G.-B. Testing gravity with CAMB and CosmoMC. *JCAP* **1108**, 005 (2011). 1106.4543.

[4] Zucca, A., Pogosian, L., Silvestri, A. & Zhao, G.-B. MGCAMB with massive neutrinos and dynamical dark energy. *JCAP* **05**, 001 (2019). 1901.05956.

[5] Lewis, A. & Bridle, S. Cosmological parameters from CMB and other data: a Monte- Carlo approach. *Phys. Rev.* **D66**, 103511 (2002). astro-ph/0205436.

[6] Crittenden, R. G., Zhao, G.-B., Pogosian, L., Samushia, L. & Zhang, X. Fables of reconstruction: controlling bias in the dark energy equation of state. *JCAP* **1202**, 048 (2012). 1112.1693.

[7] Crittenden, R. G., Pogosian, L. & Zhao, G.-B. Investigating dark energy experiments with principal components. *JCAP* **0912**, 025 (2009). astro-ph/0510293.

[8] Espejo, J. *et al.* Phenomenology of Large Scale Structure in scalar-tensor theories: joint prior covariance of $w_{\rm DE}$,

Baseline + RSD + DES	ΛCDM (reference)	No theory prior	With Horndeski prior
H_0	$(67.632)\, 67.68 \pm 0.41$	$(70.13)\, 69.3 \pm 1.5$	$(68.23)\, 67.9 \pm 1.2$
Ω_m	$(0.3115)\, 0.3107 \pm 0.0054$	$(0.2877)\, 0.293^{+0.012}_{-0.014}$	$(0.3040)\, 0.306^{+0.010}_{-0.012}$
$\langle\Sigma\rangle S_8$	$(0.8255)\, 0.822 \pm 0.010$	$(0.8236)\, 0.844^{+0.032}_{-0.037}$	$(0.8247)\, 0.838 \pm 0.025$
$\chi^2_{\rm CMB}$	2766.3	$2761.3\,(-5.0)$	$2764.4\,(-1.9)$
$\chi^2_{\rm CMBL}$	8.8	$9.3\,(+0.5)$	$8.9\,(+0.1)$
$\chi^2_{\rm SN}$	1035.0	$1029.6\,(-5.4)$	$1034.6\,(-0.4)$
$\chi^2_{\rm BAO}$	19.3	$13.8\,(-5.5)$	$17.9\,(-1.4)$
$\chi^2_{\rm DES}$	322.5	$321.3\,(-1.2)$	$322.1\,(-0.4)$
$\chi^2_{\rm tot}$	4151.8	$4135.3\,(-16.5)$	$4147.9\,(-3.9)$
	ΛCDM $+A_L$	No theory prior $+A_L$	With Horndeski prior $+A_L$
H_0	$(68.028)\, 68.20 \pm 0.46$	$(69.64)\, 69.2 \pm 1.5$	$(67.64)\, 67.7 \pm 1.3$
Ω_m	$(0.3061)\, 0.3038 \pm 0.0059$	$(0.2898)\, 0.292^{+0.012}_{-0.014}$	$(0.3071)\, 0.307 \pm 0.012$
$\langle\Sigma\rangle S_8$	$(0.8084)\, 0.800 \pm 0.013$	$(0.7672)\, 0.786 \pm 0.040$	$(0.7765)\, 0.781^{+0.031}_{-0.036}$
A_L	$(1.0777)\, 1.093^{+0.034}_{-0.038}$	$(1.219)\, 1.199^{+0.082}_{-0.096}$	$(1.248)\, 1.208 \pm 0.090$
$\chi^2_{\rm CMB}$	$2760.3\,(-6.0)$	$2760.5\,(-5.8)$	$2761.8\,(-4.5)$
$\chi^2_{\rm CMBL}$	$10.0\,(+1.2)$	$10.1\,(+1.3)$	$10.2\,(+1.4)$
$\chi^2_{\rm SN}$	$1034.8\,(-0.2)$	$1030.2\,(-4.8)$	$1034.6\,(-0.4)$
$\chi^2_{\rm BAO}$	$19.3\,(0.0)$	$12.4\,(-6.9)$	$15.1\,(-4.2)$
$\chi^2_{\rm DES}$	$321.2\,(-1.3)$	$317.8\,(-4.7)$	$319.7\,(-2.8)$
$\chi^2_{\rm tot}$	$4145.6\,(-6.2)$	$4131.0\,(-20.8)$	$4141.4\,(-10.4)$

TABLE II. The best fitting maximum posterior model parameters, in parentheses, mean and 68% C.L. constraints for the *Baseline* + RSD + DES data combination. Data likelihoods at maximum posterior are compared to their reference ΛCDM values in parenthesis.

Σ and μ in Horndeski. *Phys. Rev. D* **99**, 023512 (2019). 1809.01121.

[9] Pogosian, L. & Silvestri, A. What can Cosmology tell us about Gravity? Constraining Horndeski with Sigma and Mu. *Phys. Rev.* **D94**, 104014 (2016). 1606.05339.

[10] Joyce, A., Jain, B., Khoury, J. & Trodden, M. Beyond the Cosmological Standard Model. *Phys. Rept.* **568**, 1–98 (2015). 1407.0059.

[11] Wang, J., Hui, L. & Khoury, J. No-Go Theorems for Generalized Chameleon Field Theories. *Phys. Rev. Lett.* **109**, 241301 (2012). 1208.4612.

[12] Ade, P. A. R. *et al.* Planck 2015 results. XIV. Dark energy and modified gravity. *Astron. Astrophys.* **594**, A14 (2016). 1502.01590.

[13] Raveri, M. *et al.* A joint reconstruction of the effective dark energy and modified growth evolution with and without a Horndeski prio 2107.12990.

[14] Pinho, A. M., Casas, S. & Amendola, L. Model-independent reconstruction of the linear anisotropic stress η. *JCAP* **11**, 027 (2018). 1805.00027.

[15] Amendola, L., Kunz, M., Motta, M., Saltas, I. D. & Sawicki, I. Observables and unobservables in dark energy cosmologies. *Phys. Rev. D* **87**, 023501 (2013). 1210.0439.

[16] Bloomfield, J. K., Flanagan, E. E., Park, M. & Watson, S. Dark energy or modified gravity? An effective field theory approach. *JCAP* **1308**, 010 (2013). 1211.7054.

[17] Gleyzes, J., Langlois, D., Piazza, F. & Vernizzi, F. Essential Building Blocks of Dark Energy. *JCAP* **1308**, 025 (2013). 1304.4840.

[18] Raveri, M. Reconstructing Gravity on Cosmological Scales. *Phys. Rev. D* **101**, 083524 (2020). 1902.01366.

[19] Park, M., Raveri, M. & Jain, B. Reconstructing Quintessence. *Phys. Rev. D* **103**, 103530 (2021). 2101.04666.

[20] Moss, A., Copeland, E., Bamford, S. & Clarke, T. A model-independent reconstruction of dark energy to very high redshift (2021). 2109.14848.

[21] Aghanim, N. *et al.* Planck 2018 results. V. CMB power spectra and likelihoods (2019). 1907.12875.

[22] Alam, S. *et al.* The Completed SDSS-IV extended Baryon Oscillation Spectroscopic Survey: Cosmological Implications from two Decades of Spectroscopic Surveys at the Apache Point observatory (2020). 2007.08991.

[23] Zhao, G.-B. *et al.* The Completed SDSS-IV extended Baryon Oscillation Spectroscopic Survey: a multi-tracer analysis in Fourier space for measuring the cosmic structure growth and expansion rate (2020). 2007.09011.

[24] Wang, Y. *et al.* The clustering of the SDSS-IV extended Baryon Oscillation Spectroscopic Survey DR16 luminous red galaxy and emission line galaxy samples: cosmic distance and structure growth measurements using multiple tracers in configuration space (2020). 2007.09010.

[25] Hou, J. *et al.* The Completed SDSS-IV extended Baryon Oscillation Spectroscopic Survey: BAO and RSD measurements from anisotropic clustering analysis of the Quasar Sample in configuration space between redshift 0.8 and 2.2. *Mon. Not. Roy. Astron. Soc.* **500**, 1201–1221 (2020). 2007.08998.

[26] du Mas des Bourboux, H. *et al.* The Completed SDSS-IV extended Baryon Oscillation Spectroscopic Survey: Baryon acoustic oscillations with Lyman-α forests (2020). 2007.08995.

Baseline + RSD + DES $+M_{SN}$	ΛCDM (reference)	No theory prior	With Horndeski prior
H_0	$(68.039)\, 68.13 \pm 0.40$	$(71.34)\, 70.9 \pm 1.4$	$(69.44)\, 69.2 \pm 1.3$
Ω_m	$(0.3062)\, 0.3050 \pm 0.0052$	$(0.2759)\, 0.281 \pm 0.011$	$(0.2942)\, 0.296 \pm 0.012$
$\langle\Sigma\rangle S_8$	$(0.8107)\, 0.8134 \pm 0.0099$	$(0.8192)\, 0.836^{+0.031}_{-0.037}$	$(0.8365)\, 0.830 \pm 0.025$
$\chi^2_{\rm CMB}$	2768.4	$2763.8\,(-4.6)$	$2764.0\,(-4.4)$
$\chi^2_{\rm CMBL}$	10.1	$8.8\,(-1.3)$	$9.0\,(-1.1)$
$\chi^2_{\rm SN}$	1025.9	$1022.9\,(-3.0)$	$1025.8\,(-0.1)$
$\chi^2_{\rm BAO}$	19.5	$15.5\,(-4.0)$	$20.6\,(+1.1)$
$\chi^2_{\rm DES}$	321.2	$319.2\,(-2.0)$	$321.5\,(+0.3)$
$\chi^2_{\rm M}$	18.8	$11.9\,(-6.9)$	$12.9\,(-5.9)$
$\chi^2_{\rm tot}$	4163.9	$4142.1\,(-21.8)$	$4153.8\,(-10.1)$
	ΛCDM $+A_L$	No theory prior $+A_L$	With Horndeski prior $+A_L$
H_0	$(68.566)\, 68.71 \pm 0.44$	$(70.96)\, 70.8 \pm 1.4$	$(69.67)\, 69.1 \pm 1.4$
Ω_m	$(0.2992)\, 0.2974 \pm 0.0056$	$(0.2780)\, 0.280^{+0.011}_{-0.012}$	$(0.2935)\, 0.295 \pm 0.013$
$\langle\Sigma\rangle S_8$	$(0.7922)\, 0.789 \pm 0.013$	$(0.7584)\, 0.782 \pm 0.040$	$(0.7802)\, 0.780 \pm 0.033$
A_L	$(1.1067)\, 1.110 \pm 0.037$	$(1.209)\, 1.190^{+0.080}_{-0.096}$	$(1.118)\, 1.190^{+0.085}_{-0.099}$
$\chi^2_{\rm CMB}$	$2760.7\,(-7.7)$	$2762.1\,(-6.3)$	$2762.1\,(-6.3)$
$\chi^2_{\rm CMBL}$	$10.1\,(0.0)$	$9.8\,(-0.3)$	$10.0\,(-0.1)$
$\chi^2_{\rm SN}$	$1025.8\,(-0.1)$	$1021.6\,(-4.3)$	$1025.7\,(-0.2)$
$\chi^2_{\rm BAO}$	$20.7\,(+1.2)$	$14.6\,(-4.9)$	$19.8\,(+0.3)$
$\chi^2_{\rm DES}$	$320.2\,(-1.0)$	$317.6\,(-3.6)$	$319.2\,(-2.0)$
$\chi^2_{\rm M}$	$15.8\,(-3.0)$	$12.4\,(-6.4)$	$13.0\,(-5.8)$
$\chi^2_{\rm tot}$	$4153.3\,(-10.6)$	$4138.1\,(-25.8)$	$4149.8\,(-14.1)$

TABLE III. The best fitting maximum posterior model parameters, in parentheses, mean and 68% C.L. constraints for the *Baseline* + RSD + DES + M_{SN} data combination. Data likelihoods at maximum posterior are compared to their reference ΛCDM values in parenthesis.

[27] Ross, A. J. *et al.* The clustering of the SDSS DR7 main Galaxy sample – I. A 4 per cent distance measure at $z = 0.15$. *Mon. Not. Roy. Astron. Soc.* **449**, 835–847 (2015). 1409.3242.

[28] Beutler, F. *et al.* The 6dF Galaxy Survey: Baryon Acoustic Oscillations and the Local Hubble Constant. *Mon. Not. Roy. Astron. Soc.* **416**, 3017–3032 (2011). 1106.3366.

[29] Zhao, G.-B. *et al.* The clustering of galaxies in the completed SDSS-III Baryon Oscillation Spectroscopic Survey: tomographic BAO analysis of DR12 combined sample in Fourier space. *Mon. Not. Roy. Astron. Soc.* **466**, 762–779 (2017). 1607.03153.

[30] Scolnic, D. *et al.* The Complete Light-curve Sample of Spectroscopically Confirmed SNe Ia from Pan-STARRS1 and Cosmological Constraints from the Combined Pantheon Sample. *Astrophys. J.* **859**, 101 (2018). 1710.00845.

[31] Bautista, J. E. *et al.* The Completed SDSS-IV extended Baryon Oscillation Spectroscopic Survey: measurement of the BAO and growth rate of structure of the luminous red galaxy sample from the anisotropic correlation function between redshifts 0.6 and 1. *Mon. Not. Roy. Astron. Soc.* **500**, 736–762 (2020). 2007.08993.

[32] de Mattia, A. *et al.* The Completed SDSS-IV extended Baryon Oscillation Spectroscopic Survey: measurement of the BAO and growth rate of structure of the emission line galaxy sample from the anisotropic power spectrum between redshift 0.6 and 1.1. *Mon. Not. Roy. Astron. Soc.* **501**, 5616–5645 (2021). 2007.09008.

[33] Neveux, R. *et al.* The completed SDSS-IV extended Baryon Oscillation Spectroscopic Survey: BAO and RSD measurements from the anisotropic power spectrum of the quasar sample between redshift 0.8 and 2.2. *Mon. Not. Roy. Astron. Soc.* **499**, 210–229 (2020). 2007.08999.

[34] Abbott, T. M. C. *et al.* Dark Energy Survey year 1 results: Cosmological constraints from galaxy clustering and weak lensing. *Phys. Rev.* **D98**, 043526 (2018). 1708.01530.

[35] Riess, A. G. *et al.* Cosmic Distances Calibrated to 1% Precision with Gaia EDR3 Parallaxes and Hubble Space Telescope Photometry of 75 Milky Way Cepheids Confirm Tension with ΛCDM. *Astrophys. J. Lett.* **908**, 6 (2021). 2012.08534.

[36] Benevento, G., Hu, W. & Raveri, M. Can Late Dark Energy Transitions Raise the Hubble constant? *Phys. Rev. D* **101**, 103517 (2020). 2002.11707.

[37] Barreira, A., Sánchez, A. G. & Schmidt, F. Validating estimates of the growth rate of structure with modified gravity simulations. *Phys. Rev. D* **94**, 084022 (2016). 1605.03965.

[38] Bose, B., Koyama, K., Hellwing, W. A., Zhao, G.-B. & Winther, H. A. Theoretical accuracy in cosmological growth estimation. *Phys. Rev. D* **96**, 023519 (2017). 1702.02348.

[39] Calabrese, E., Slosar, A., Melchiorri, A., Smoot, G. F. &

Zahn, O. Cosmic Microwave Weak lensing data as a test for the dark universe. *Phys. Rev. D* **77**, 123531 (2008). 0803.2309.

[40] Silvestri, A., Pogosian, L. & Buniy, R. V. Practical approach to cosmological perturbations in modified gravity. *Phys. Rev.* **D87**, 104015 (2013). 1302.1193.

[41] Peirone, S., Koyama, K., Pogosian, L., Raveri, M. & Silvestri, A. Large-scale structure phenomenology of viable Horndeski theories. *Phys. Rev.* **D97**, 043519 (2018). 1712.00444.

[42] Gleyzes, J., Langlois, D., Mancarella, M. & Vernizzi, F. Effective Theory of Dark Energy at Redshift Survey Scales. *JCAP* **1602**, 056 (2016). 1509.02191.

[43] Saltas, I. D., Sawicki, I., Amendola, L. & Kunz, M. Anisotropic Stress as a Signature of Nonstandard Propagation of Gravitational Waves. *Phys. Rev. Lett.* **113**, 191101 (2014). 1406.7139.

[44] Abbott, B. *et al.* GW170817: Observation of Gravitational Waves from a Binary Neutron Star Inspiral. *Phys. Rev. Lett.* **119**, 161101 (2017). 1710.05832.

[45] Abbott, B. P. *et al.* Gravitational Waves and Gamma-rays from a Binary Neutron Star Merger: GW170817 and GRB 170817A. *Astrophys. J.* **848**, L13 (2017). 1710.05834.

[46] Deffayet, C., Esposito-Farese, G. & Vikman, A. Covariant Galileon. *Phys. Rev. D* **79**, 084003 (2009). 0901.1314.

[47] Deffayet, C., Pujolas, O., Sawicki, I. & Vikman, A. Imperfect Dark Energy from Kinetic Gravity Braiding. *JCAP* **1010**, 026 (2010). 1008.0048.

[48] Linder, E. V. No Slip Gravity. *JCAP* **03**, 005 (2018). 1801.01503.